

Ternary Spiking Neural Networks Enhanced by Complemented Neurons and Membrane Potential Aggregation

Boxuan Zhang ^{*1} Jiaxin Wang ^{*1} Zhen Xu ² Kuan Tao ¹

Abstract

Spiking Neural Networks (SNNs) are promising energy-efficient models and powerful frameworks of modeling neuron dynamics. However, existing binary spiking neurons exhibit limited biological plausibilities and low information capacity. Recently developed ternary spiking neuron possesses higher consistency with biological principles (i.e. excitation-inhibition balance mechanism). Despite of this, the ternary spiking neuron suffers from defects including iterative information loss, temporal gradient vanishing and irregular distributions of membrane potentials. To address these issues, we propose Complemented Ternary Spiking Neuron (CTSN), a novel ternary spiking neuron model that incorporates an learnable complemental term to store information from historical inputs. CTSN effectively improves the deficiencies of ternary spiking neuron, while the embedded learnable factors enable CTSN to adaptively adjust neuron dynamics, providing strong neural heterogeneity. Furthermore, based on the temporal evolution features of ternary spiking neurons' membrane potential distributions, we propose the Temporal Membrane Potential Regularization (TMPr) training method. TMPr introduces time-varying regularization strategy utilizing membrane potentials, furhter enhancing the training process by creating extra backpropagation paths. We validate our methods through extensive experiments on various datasets, demonstrating remarkable performance advances.

1. Introduction

Spiking Neural Networks (SNNs) (Maass, 1997) have received widespread attention in recent years (Roy et al., 2019;

^{*}Equal contribution ¹School of Sports Engineering, Beijing Sport University, Beijing, China ²School of Mathematics, Statistics and Mechanics, Beijing University of Technology, Beijing, China. Correspondence to: Kuan Tao <taokuan@bsu.edu.cn>.

Submitted manuscript. January 23, 2026.

Schuman et al., 2022; Kuditipudi et al., 2025). Inspired by the biological neurons, SNNs adopt spiking neurons such as the Leaky Integrate-and-Fire (LIF) model (Gerstner et al., 2014), realizing information transmission through binary spike-driven communication. This spike-driven communication equips SNNs multiplication-free characteristic and sparsity in information processing, offering SNNs excellent computational efficiency and low power consumption, making them powerful frameworks for modeling biological neural networks (Schmidt et al., 2018; Siegle et al., 2021). Spiking neuron models typically implement binary spiking mechanism, which allows neurons to fire spikes with values of either 0 or 1. This two-state characteristic of binary spiking mechanism constrains SNNs' information capacity. Moreover, binary spiking mechanism limits the potential of SNNs to simulate complex behaviors observed in biological neurons, such as excitation-inhibition balance mechanism (Turrigiano, 2008). Previous study (Guo et al., 2024) proposed a ternary spiking neuron model that fires spikes in $\{-1, 0, 1\}$. Ternary spiking neuron possesses higher consistency with biological principles (see Appendix. A) and greater information capacity while retaining the multiplication-free and event-driven features, effectively elevates SNNs' performance. To gain a deeper understanding of this model, we perform in-depth analysis in Section. 4, revealing its existing deficiencies including iterative information loss, temporal gradient vanishing and irregular distributions of membrane potentials. Besides, the current form of ternary spiking neuron neglects the heterogeneity of neuron dynamics (Yao et al., 2022; Zheng et al., 2024), which is one of the primary factors leading to suboptimal performance of SNNs. In this case, further discussions and modifications are required to unleash the potential of this promising neuron model.

In this paper, we propose the Complemented Ternary Spiking Neuron (CTSN) model. In CTSN, we introduce a learnable complemental term $h(t)$ in the integration process, which can adaptively capture and maintain information from historical inputs, equipping neurons with stronger heterogeneity. CTSN continuously reinjects the information contained in previous inputs to the membrane potential as timestep increases, creates extra backpropagation paths in temporal gradient computation, and smooths the distribution of

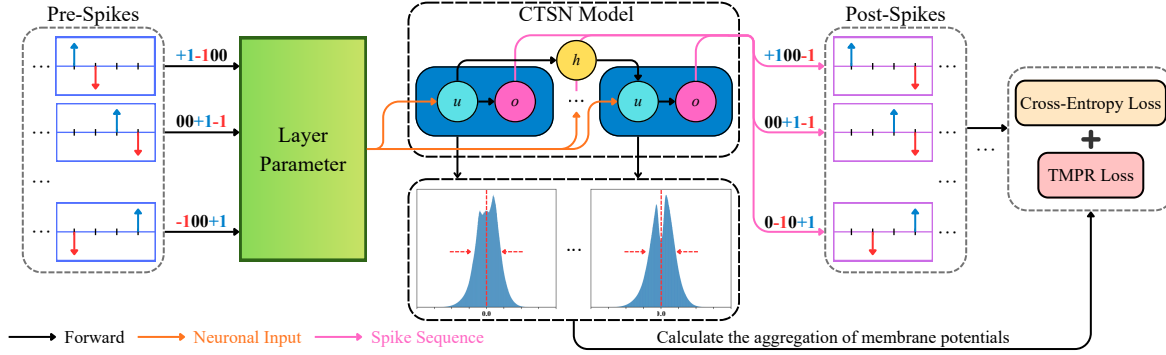


Figure 1. The overall workflow of CTSN and TMPR.

membrane potential.

By analyzing the temporal evolution of ternary spiking neuron’s membrane potential distribution, we propose the Temporal Membrane Potential Regularization (TMPR) training method. TMPR introduces a spatio-temporal regularization strategy that exploits the aggregation degree of membrane potentials across multilayers and timesteps, further enhances the gradient flow in backpropagation stage. Under the joint promotion of CTSN and TMPR, the performance of ternary SNNs are effectively elevated. Figure. 1 depicts the workflow of our methods. Our main contributions are:

- We propose the CTSN model with a learnable complemental integration term to preserve historical information to improve temporal gradient propagation, mitigates iterative information loss and smooths irregular membrane potential distributions.
- We introduce the TMPR training method that exploits the aggregation degree of membrane potentials across layers and timesteps as additional regularization terms, enhancing gradient flow of ternary SNNs during training.
- We validate the effectiveness of our methods through extensive experiments¹ and demonstrate significant improvements over existing SNN methods on various tasks.

2. Related Work

Variants of Spiking Neuron Models. Multiple variants of spiking neuron models are proposed in previous studies and these models can be divided into two categories: binary and multi-nary. Various binary neuron models with enhanced neuron dynamics are developed in prior works (Fang et al., 2021b; Yao et al., 2022; Wang et al., 2022; Huang et al., 2024). In parallel, binary spiking neurons with bio-inspired

structures such as multi-branch (Zheng et al., 2024) and multi-compartment (Capone et al., 2023; Feng et al., 2025a) have been proposed for modeling specific tasks (i.e. long sequence modeling). Despite their high biological plausibility and outstanding performance on their designed tasks, these models not only introduce significant computational complexity but also cannot be generalized to various network backbones and general scenarios. To increase the representation space of spiking neurons, recent works propose neuron models with multi-nary spiking mechanism for extending the binary spike space $\{0, 1\}$ to a wider range. Sun et al. (2022) proposed a neuron model that emits $\{0, 1, 2\}$ spikes. This model increases the information bandwidth of spike sequence, but fails to enjoy multiplication-free characteristic, resulting in lower energy efficiency. Wang et al. (2025) proposed a multi-branch multi-compartment neuron model with the integer set as its spike space. However, this model is specifically designed for long sequence modeling, with poor generalizability and high computational complexity. Guo et al. (2024) developed the ternary spiking neuron model for image classification tasks. However, the improvement to SNNs by merely expanding spike spaces is limited. In this paper, our CTSN incorporates bio-inspired neuron behaviors and $\{-1, 0, 1\}$ ternary spiking mechanism to advance the performance of SNNs without adding significant complexity to the neuron.

Gradient-based Learning of SNNs. Gradient-based learning of SNNs follows the idea of backpropagation in ANN (Rumelhart et al., 1986), which essentially treats SNNs as RNNs and directly trains them via surrogate gradients (Neftci et al., 2019) and backpropagation through time (BPTT) Wu et al. (2018) frameworks. During the forward stage, spikes are emitted by the non-differentiable spiking function, while the non-differentiable terms are generally replaced by surrogate gradients in backpropagation. In order to further improve the efficiency of direct training, innovative approaches (Wu et al., 2019; Fang et al., 2021a; Deng et al., 2022; Meng et al., 2023; Shen et al., 2024; Liu et al., 2025; Ding et al., 2025; Zhang et al., 2026) are proposed to

¹<https://github.com/ZBX05/Enhanced-TernarySNN>

accelerate the convergence of SNNs. Besides, some studies (Mukhoty et al., 2023; Wang et al., 2023) focus on surrogate gradient to improve the accuracy of SNNs. However, few works link the training process directly with neuron dynamics. Zheng et al. (2021b) proposed tdbN, which combines neuron threshold with batch normalization for efficient training. Guo et al. (2023) utilized membrane potentials as regularization terms to reduce the quantization error of SNNs. Still, these works neglect the inherent temporal characteristics of neuron dynamics. In this paper, we construct time-varying regularization strategy aligned with the temporal evolution of membrane potential distributions to constrain membrane potentials and mitigate temporal gradient vanishing.

3. Preliminary

We adopt the ternary spiking neuron model proposed in (Guo et al., 2024) as the baseline ternary neuron model due to its event-driven and multiplication-free features, which is described as

$$u(t) = \tau u(t-1)(1 - |o(t-1)|) + x(t), \quad (1)$$

$$x(t) = \sum_{l=1}^L \mathbf{W}^l o^{l-1}(t) + b^l, \quad (2)$$

and

$$o(t) = \Theta(u(t), V_{th}) = \begin{cases} 1, & \text{if } u(t) \geq V_{th} \\ -1, & \text{if } u(t) \leq -V_{th} \\ 0, & \text{otherwise} \end{cases}, \quad (3)$$

where l is the layer index, V_{th} is the firing threshold, and τ is the time constant. The membrane potential $u(t)$ is updated at each timestep t based on the previous membrane potential $u(t-1)$ and input $x(t)$, which is produced by the l^{th} weight matrix \mathbf{W}^l , bias term b^l , and spikes of the previous layer neuron $o^{l-1}(t)$. The neuron fires when $u(t) \geq V_{th}$ or $u(t) \leq -V_{th}$, and the membrane potential will be reset to 0 after firing, which is known as the hard reset.

The network's final output at t^{th} timestep is $O(t) = \phi(\mathbf{X}(t))$, where ϕ denotes the network and \mathbf{X} is the external input sequence. The prediction is based on the average output over all timesteps $\frac{1}{T} \sum_{t=1}^T O(t)$, where $T > 0$. The loss function is defined as

$$\mathcal{L} = \ell\left(\frac{1}{T} \sum_{t=1}^T O(t), \mathbf{Y}\right), \quad (4)$$

where \mathbf{Y} is the label, and ℓ represents the cross-entropy loss function.

Since the spike activity is not differentiable, we use a rectangular-shaped surrogate gradient function to calculate the spike derivative:

$$\frac{\partial o(t)}{\partial u(t)} \approx \mathbb{H}(u(t)) = \text{Sign}(|u(t)| - V_{th} < a), \quad (5)$$

where $\text{Sign}(\cdot)$ denotes the sign function and a is a hyperparameter controlling the width. In this work, we set $a = V_{th} = 0.5$.

4. Motivation

4.1. Iterative Information Loss of Ternary Spiking Neuron

SNN can be seen as a special case of RNN, where the hidden state is the membrane potential $u(t)$. From this perspective, inspired by the iterative firing process of binary spiking neurons (Huang et al., 2025), the ternary spiking neuron model depicted by Eq. 1 - 3 can be derived into

$$\begin{aligned} o(t) &= \Theta(u(t), V_{th}) \\ &= \Theta(\tau u(t-1)(1 - |o(t-1)|) + x(t), V_{th}) \\ &= \Theta\left(\tau(1 - |o(t-1)|)(\tau(1 - |o(t-2)|)u(t-2) \right. \\ &\quad \left. + x(t-1)) + x(t), V_{th}\right) \\ &\quad \dots \\ &= \Theta\left(x(t) + \sum_{i=1}^{t-1} \left(\tau^{t-i} x(i) \prod_{j=i}^{t-1} (1 - |o(j)|)\right), V_{th}\right), \end{aligned} \quad (6)$$

where $\Theta(\cdot, V_{th})$ denotes the firing process described in Eq. 3. From Eq. 6, it saliently yields that firing status of a ternary spiking neuron is highly related to the inputs and spikes in previous timesteps. Due to the hard reset mechanism, the information stored in previous inputs is lost after each firing. Therefore, similar to binary spiking neurons with hard reset, the ternary spiking neuron model is a memoryless model. Once the neuron fires a spike at a given timestep, it will be unable to utilize any information from the inputs arrived in previous timesteps. For binary spiking neurons, the soft reset mechanism (Guo et al., 2022) is generally implemented to address this issue. We conducted experiments to test the soft reset mechanism on ternary spiking neuron, however, the accuracy results turn out to be unsatisfactory (results and detailed analysis are in Appendix. B).

4.2. Temporal Gradient Vanishing in Ternary Spiking Neuron

Ternary SNNs are trained through BPTT (Wu et al., 2018). Similar to binary SNNs (Meng et al., 2023; Huang et al.,

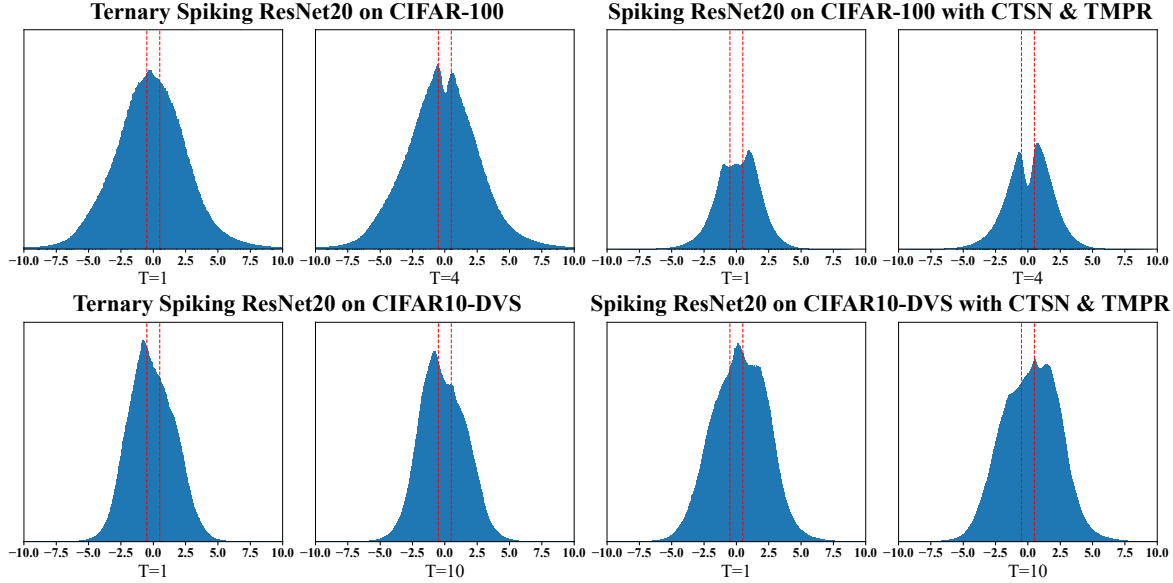


Figure 2. Membrane potential distributions of the first and the last timestep. Upper left: Ternary spiking ResNet20 on CIFAR-100 (4 timesteps). Lower left: Ternary spiking ResNet20 on CIFAR10-DVS (10 timesteps). Upper right: Spiking ResNet20 on CIFAR-100 (4 timesteps) with CTSN and TMPR. Lower right: Spiking ResNet20 on CIFAR10-DVS (10 timesteps) with CTSN and TMPR. See Appendix. D for detailed visualizations.

2024), the backpropagation process of gradients involves the temporal dimension, which can be described as

$$\begin{aligned}
 \frac{\partial \mathcal{L}}{\partial \mathbf{W}^l} &= \sum_{t=1}^T \frac{\partial \mathcal{L}}{\partial u^l(t)} \frac{\partial u^l(t)}{\partial \mathbf{W}^l} \\
 &= \sum_{t=1}^T \left(\nabla_{u^l} \mathcal{P}(t) + \nabla_{u^l} \mathcal{T}(t) \right) \frac{\partial u^l(t)}{\partial \mathbf{W}^l} \\
 &= \sum_{t=1}^T \left(\underbrace{\frac{\partial \mathcal{L}}{\partial o^l(t)} \frac{\partial o^l(t)}{\partial u^l(t)}}_{\nabla_{u^l} \mathcal{P}(t)} \right. \\
 &\quad \left. + \underbrace{\sum_{t'=t+1}^T \frac{\partial \mathcal{L}}{\partial o^l(t')} \frac{\partial o^l(t')}{\partial u^l(t')} \prod_{t''=1}^{t'-t} \epsilon^l(t' - t'')}_{\nabla_{u^l} \mathcal{T}(t)} \right) \frac{\partial u^l(t)}{\partial \mathbf{W}^l}, \tag{7}
 \end{aligned}$$

where $l = L, L-1, \dots, 1, t' \in [t+1, T]$. For different layers, $\frac{\partial \mathcal{L}}{\partial o^l(t)}$ term is expressed in different forms, which is calculated as

$$\frac{\partial \mathcal{L}}{\partial o^l(t)} = \begin{cases} \frac{\partial \mathcal{L}}{\partial o^L(t)}, & l = L \\ \frac{\partial \mathcal{L}}{\partial u^{l+1}(t)} \frac{\partial u^{l+1}(t)}{\partial o^l(t)}, & L = L-1, L-2 \dots 1 \end{cases}. \tag{8}$$

$\epsilon^l(t)$ is defined as

$$\begin{aligned}
 \epsilon^l(t) &= \frac{\partial u^l(t+1)}{\partial u^l(t)} + \frac{\partial u^l(t+1)}{\partial |o^l(t)|} \frac{\partial |o^l(t)|}{\partial u^l(t)} \\
 &= \tau(1 - |o^l(t)| - \text{Sign}(o^l(t))u^l(t)\mathbb{H}[u^l(t)]). \tag{9}
 \end{aligned}$$

In this case, we obtain

$$\nabla_{\mathbf{u}^l} \mathcal{T}(t) = \sum_{t'=t+1}^T \frac{\partial \mathcal{L}}{\partial o^l(t')} \frac{\partial o^l(t')}{\partial u^l(t')} \underbrace{\tau^{t'-t}}_{\text{Part I}} \prod_{t''=1}^{t'-t} \underbrace{\kappa^l(t' - t'')}_{\text{Part II}}. \tag{10}$$

where term $\mathbb{H}(\cdot)$ denotes the rectangle-shaped surrogate gradient we used in this work. The detailed derivations are given in Appendix. C. For **Part I**, since the time constant τ is usually smaller than 1 (e.g. $\tau = 0.5$ (Du et al., 2025) and $\tau = 0.25$ (Zheng et al., 2021a)), $\tau^{t'-t}$ eventually converges to 0 as $(t' - t)$ increases. Therefore, the diagonal values of matrix $\prod_{t''=1}^{t'-t} \epsilon^l(t' - t'')$ are smaller than the single term $\epsilon^l(t' - t'')$, causing the vanishment of temporal gradients in early timesteps (Meng et al., 2023). **Part II** can be expressed as

$$\kappa^l(t) = \begin{cases} \tau u^l(t), & -\frac{3}{2}V_{th} \leq u^l(t) < -V_{th} \\ \tau(1 + u^l(t)), & -V_{th} \leq u^l(t) < 0 \\ \tau(1 - u^l(t)), & 0 < u^l(t) \leq V_{th} \\ \tau(-1 + u^l(t)), & V_{th} < u^l(t) \leq \frac{3}{2}V_{th} \\ 0, & \text{otherwise} \end{cases}. \tag{11}$$

From Eq. 11, it is deduced that $\kappa^l(t) = 0$ always holds when $|u(t)| \geq \frac{3}{2}V_{th}$, even if the neuron actually fires a spike. In other words, within the temporal range of $(t+1, T)$, as long as the neuron fires at least once under the condition of $|u(t)| \geq \frac{3}{2}V_{th}$, the corresponding temporal gradient will

vanish. This is an unavoidable issue in the ternary spiking neuron.

4.3. Irregular Membrane Potential Distribution of Ternary Spiking Neuron

As can be seen from Figure 2, the membrane potential distributions of the ternary spiking neuron exhibits distinct characteristics across different types of data. This phenomenon is most likely attributed to the inherent sparsity of neuromorphic data. On static image data, the membrane potential distribution exhibit irregular and threshold-deviated bimodal pattern as the timestep increases. This may lead to over activation, resulting in gradient vanishing as described in Eq. 11. In contrast, for neuromorphic data, the membrane potential at later timesteps becomes more sharply peaked but does not display a distinct bimodal distribution. This may result in a large number of neurons remaining silent, thereby degrading the representational power of neurons. Detailed visualizations are provided in Appendix. D. Therefore, tailored approaches are required to address the irregular membrane potential distribution of ternary spiking neurons on different data types.

5. Methodology

5.1. Complemented Ternary Spiking Neuron

Inspired by biological principles (see Appendix. A), we propose to add an additional term to the ternary spiking neuron model. The complemented ternary spiking neuron (CTSN) can be described by

$$u(t) = \tau \tilde{u}(t-1)(1 - |o(t-1)|), \quad (12)$$

$$h(t) = \mathbb{G}(h(t-1), u(t), \alpha, \beta, \gamma), \quad (13)$$

$$\tilde{u}(t) = h(t) + x(t), \quad (14)$$

and

$$o(t) = \Theta(\tilde{u}(t), V_{th}). \quad (15)$$

Term $\tilde{u}(t)$ denotes the membrane potential after integration, and $h(t)$ is the additional term. The initial value of $\tilde{u}(t)$ and $h(t)$ are 0. Function $\mathbb{G}(h(t-1), u(t), \alpha, \beta, \gamma)$ defines the update process of the complemental membrane potential. For static image data, $\mathbb{G}(h(t-1), u(t), \alpha, \beta, \gamma)$ is defined as

$$\mathbb{G} = \begin{cases} \alpha h(t-1) + \gamma u(t), & h(t-1) \geq 0 \\ \beta h(t-1) + \gamma u(t), & h(t-1) < 0 \end{cases}. \quad (16)$$

For neuromorphic data, $\mathbb{G}(h(t-1), u(t), \alpha, \beta, \gamma)$ is defined as

$$\mathbb{G} = \begin{cases} \alpha h(t-1) + \beta u(t), & u(t) \geq 0 \\ \alpha h(t-1) + \gamma u(t), & u(t) < 0 \end{cases}. \quad (17)$$

α, β, γ are learnable parameters. To ensure all these parameters are constrained in $(0, 1)$, we train parameters $\omega_\alpha, \omega_\beta, \omega_\gamma$ and set

$$\alpha = \text{Sigmoid}(\omega_\alpha), \beta = \text{Sigmoid}(\omega_\beta), \gamma = \text{Sigmoid}(\omega_\gamma), \quad (18)$$

with $\omega_\alpha, \omega_\beta, \omega_\gamma$ setting to 0 by default. In this case, the initial values of α, β, γ are 0.5.

The additional term $h(t)$ can be seen as a memristor without any reset mechanism. For those neurons that intermittently emit spikes, $h(t)$ can effectively retain information from inputs arrived in previous timesteps, and reinject these information to the neuron in later timesteps, thereby partially addressing the iterative information loss problem discussed in Section. 4.1. Moreover, $h(t)$ also smooths the membrane potential and contributes the temporal gradient during backpropagation. The pseudo-code for the CTSN model is provided in Appendix. E.1.

5.2. Temporal Membrane Potential Regularization

As observed from the Figure 2, the membrane potential of ternary spiking neurons inevitably differentiate into irregular distributions (i.e. bimodal distribution) as the timestep increases. In this case, we utilize the aggregation degree of the membrane potential as a regular term to enhance the training process, which is called Temporal Membrane Potential Regularization (TMPr) training method. TMPr is described as

$$\mathcal{L} = \mathcal{L}_{CE} + \mathcal{L}_{TMPr}, \quad (19)$$

$$\mathcal{L}_{TMPr} = \frac{1}{TL} \sum_{t=1}^T \frac{\lambda}{t} \sum_{l=1}^L \frac{[\tilde{u}^l(t)]^2}{BD^l}, \quad (20)$$

where B denotes the batch size, D^l denotes the length of the l^{th} layer's neuron membrane potential $\tilde{u}^l(t)$ (for image data which in the shape of $[C, H, W]$, we can flatten the membrane potential so that it becomes a vector, in this case $D^l = C^l \times H^l \times W^l$), T denotes the total timesteps, L denotes the total number of layers, λ is a regularization coefficient.

TMPr utilizes $\tilde{u}(t)^2$ to measure the aggregation degree of membrane potential. The strength of regularization is jointly controlled by the time step t and λ . For early timesteps, it is necessary to impose strong regularization to force the membrane potential gathering around 0. Since the membrane potential will inevitably differentiate into irregular distribution in later time steps, we propose to reduce the strength of regularization to avoid the unstable training process caused by excessive penalties. This mechanism aligns with the temporal evolution trend of membrane potential distribution. The pseudo-code for the TMPr training method is provided in Appendix. E.2.

Table 1. Ablation study results of the proposed method (%). w/ C: with CTSN. w/ C&T: with CTSN & TMPR.

Dataset	T	Method		
		Ternary	w/ C	w/ C&T
CIFAR-100	4	73.95	74.18	74.82
	6	74.12	74.48	75.12
CIFAR10-DVS	10	80.30	80.57	81.23

5.3. Gradient Analysis of CTSN and TMPR

With the implementation of CTSN and TMPR, the backpropagation process of gradients can be calculated as

$$\frac{\partial \mathcal{L}}{\partial \mathbf{W}^l} = \sum_{t=1}^T \left(\underbrace{\frac{\partial \mathcal{L}_{CE}}{\partial \tilde{u}^l(t)}}_{\text{Part I}} + \underbrace{\frac{\partial \mathcal{L}_{TMPR}}{\partial \tilde{u}^l(t)}}_{\text{Part II}} \right) \frac{\partial \tilde{u}^l(t)}{\partial \mathbf{W}^l}. \quad (21)$$

From Eq. 20, we can calculate **Part I** as

$$\frac{\partial \mathcal{L}_{CE}}{\partial \tilde{u}^l(t)} = \nabla_{\tilde{u}^l} \mathcal{P}(t) + \nabla_{\tilde{u}^l} \mathcal{T}(t). \quad (22)$$

The $\nabla_{\tilde{u}^l} \mathcal{P}(t)$ shares the same form with the counterpart in ternary spiking neuron in Eq. 7. The $\nabla_{\tilde{u}^l} \mathcal{T}(t)$ can be expanded as

$$\begin{aligned} \nabla_{\tilde{u}^l} \mathcal{T}(t) &= \frac{\partial \mathcal{L}}{\partial o^l(t+1)} \frac{\partial o^l(t+1)}{\partial \tilde{u}^l(t+1)} \xi^l(t) \\ &+ \sum_{t'=t+2}^T \frac{\partial \mathcal{L}}{\partial o^l(t')} \frac{\partial o^l(t')}{\partial \tilde{u}^l(t')} \prod_{t''=1}^{t'-t} \left(\xi^l(t' - t'') + \nabla_{h^l} \mathbb{G}^l \right). \end{aligned} \quad (23)$$

where $\nabla_{h^l} \mathbb{G}^l$ denotes the temporal gradient $\frac{\partial h^l(t+1)}{\partial h^l(t)}$, and $\xi^l(t)$ is defined as

$$\begin{aligned} \xi^l(t) &= \frac{\partial h^l(t+1)}{\partial \tilde{u}^l(t)} + \frac{\partial h^l(t+1)}{\partial |o(t)|} \frac{\partial |o(t)|}{\partial \tilde{u}^l(t)} \\ &= \nabla_{\tilde{u}^l} \mathbb{G}^l + \frac{\partial h^l(t+1)}{\partial |o(t)|} \frac{\partial |o(t)|}{\partial \tilde{u}^l(t)}, \end{aligned} \quad (24)$$

where $\nabla_{\tilde{u}^l} \mathbb{G}^l$ denotes the spatial gradient $\frac{\partial h^l(t+1)}{\partial \tilde{u}^l(t)}$. Details of the above derivations are given in Appendix F. As shown in Eq. 23, CTSN reduces to ternary spiking neuron when $T \leq 2$. When $T > 2$, the unreset term $h(t)$ generates additional backpropagation path, magnifying the temporal gradient on intermediate timesteps to against the temporal gradient vanishing induced by the product operations. We believe this additional part contributes to the advancement on performance.

Part II can be calculated as

$$\frac{\partial \mathcal{L}_{TMPR}}{\partial \tilde{u}^l(t)} = \frac{2\lambda}{tT LBD^l} \tilde{u}^l(t). \quad (25)$$

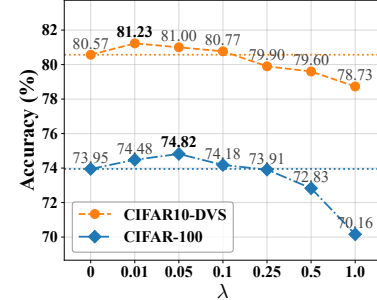


Figure 3. Influence of the hyperparameter λ on performance.

As can be seen from Eq. 25, the TMPR method introduces direct backpropagation paths to the gradient of membrane potential on each timestep and layer within the SNN, which can be viewed as residual connections with varying strength over time on both spatial and temporal dimensions, compensating for the temporal gradient vanishing problem in each layer on early timesteps (i.e. smaller t).

CTSN and TMPR jointly enhance the backpropagation of gradients in both spatial and temporal dimensions, effectively mitigating the temporal gradient vanishing problem discussed in Section 4.2. This theoretical analysis aligns with our experimental observations in Section 6, where the integration of CTSN and TMPR leads to remarkable performance improvements in ternary spiking neural networks.

6. Experimental Results

In this section, we validate the effectiveness of our proposed methods through a series of ablation studies. We perform a thorough analysis and comparison of our approach against other state-of-the-art methods using both static and neuromorphic datasets.

6.1. Ablation Studies

Effectiveness of CTSN and TMPR. In order to verify the effectiveness of our CTSN and TMPR method, we conduct experiments on CIFAR-100 and CIFAR10-DVS datasets with ResNet20 as the backbone. As listed in Table 1, the networks implemented with CTSN outperforms those using ternary spiking neurons across different timestep settings on various datasets. With the further equipments of TMPR, the classification accuracy of ResNet20 model raised from 80.57% to 81.23% on CIFAR10-DVS, 74.48% to 75.12% on CIFAR-100 when time length $T = 6$, demonstrating the effectiveness of this method. These results indicate that our CTSN and TMPR methods effectively advance the gradient-based SNN optimization.

Influence of the Hyperparameter in TMPR Method. To explore the influence of the regularization coefficient λ on

Table 2. Comparison with other state-of-the-art methods. We compare our method with the results reported in the respective literature. *: self-implementation results. †: implementation of our methods with open source code (Fang et al., 2023).

Dataset	Methods	Architecture	T	Accuracy (%)
CIFAR-10	PLIF (Fang et al., 2021b)	PLIF Net	6	94.25
	GLIF (Yao et al., 2022)	ResNet18	6	94.88
	TET (Deng et al., 2022)	ResNet19	4	94.44
	RMP-Loss (Guo et al., 2023)	ResNet19	4	95.51
	ASGL (Wang et al., 2023)	ResNet18	4	95.35
	CLIF (Huang et al., 2024)	ResNet18	4	96.01
	Ternary Spike* (Guo et al., 2024)	ResNet19	4	96.28
		ResNet20	6	94.62
Ours		ResNet19	4	96.46
		ResNet20	4	94.92
		ResNet20	6	95.01
CIFAR-100	GLIF (Yao et al., 2022)	ResNet18	6	77.35
	TET (Deng et al., 2022)	ResNet19	4	74.47
	RMP-Loss (Guo et al., 2023)	ResNet19	4	78.28
	ASGL (Wang et al., 2023)	ResNet18	4	77.74
	CLIF (Huang et al., 2024)	ResNet18	4	79.69
	Ternary Spike* (Guo et al., 2024)	ResNet19	4	79.68
		ResNet20	6	74.12
	Ours	ResNet19	4	81.19
		ResNet20	4	74.82
		ResNet20	6	75.12
ImageNet-100	LocalZO (Mukhoty et al., 2023)	SEW-ResNet34	4	81.56
	IMP+LTS (Shen et al., 2024)	SEW-ResNet34	4	80.80
	FPT (Feng et al., 2025b)	SEW-ResNet34	4	83.27
Ours		ResNet34	4	83.78
		SEW-ResNet34	4	85.06
CIFAR10-DVS	PLIF(Fang et al., 2021b)	PLIF Net	20	74.80
	GLIF (Yao et al., 2022)	7B-wideNet	16	78.10
	CLIF (Huang et al., 2024)	VGG11	16	79.00
	Ternary Spike* (Guo et al., 2024)	ResNet20	10	80.30
Ours		VGG16	10	79.06
		ResNet20	10	81.23
		VGGSNN[†]	10	83.20

the performance of the proposed TMPR method, we conduct experiments on CIFAR-100 and CIFAR10-DVS datasets, taking values set to $\{0.01, 0.05, 0.1, 0.25, 0.5, 1.0\}$. Results in Figure. 3 show that the performance of TMPR method first increases when $\lambda > 0$, and then degrades significantly when $\lambda \geq 0.25$. We argue that this is due to the fact that too large λ will cause excessive regularization in early timesteps, which dilutes the gradients generated by the classification loss \mathcal{L}_{CE} during backpropagation, providing the network with an incorrect learning direction. As a result, we set λ to 0.05 for CIFAR-10/100 and ImageNet-100, 0.01 for

CIFAR10-DVS.

Temporal Ablation of CTSN. To validate the effectiveness of CTSN on magnifying the temporal gradient, we verify the performance comparison between CTSN and the ternary spiking neuron with various timesteps. The experiment is conducted on CIFAR-100 with ResNet20 as the backbone. The results are demonstrated in Figure. 4. When the total timestep is set to 2, our proposed CTSN model cannot magnify the temporal gradient and yield accuracy around 73.4% similar to the ternary spiking neuron. As the timestep in-

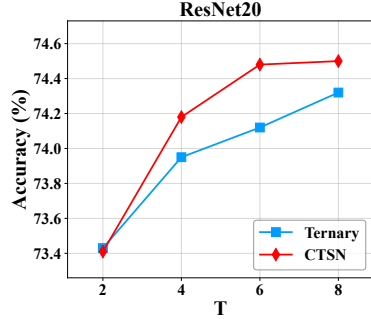


Figure 4. Timestep ablation study of CTSN.

creases, CTSN consistently outperforms the ternary spiking neuron, indicating that the complemented term in CTSN contributes to the temporal gradient. This is consistent with the gradient analysis in Section 5.3.

Learnable Parameters Tracking. As shown in Eq. 16 and Eq. 17, our CTSN model contains three learnable parameters. We visualize the learnable parameters of each layer in ResNet20 (without TMPR) on CIFAR-100 and CIFAR10-DVS datasets. As described in Section 5.1, the initial values of α, β, γ are all set to 0.5. As shown in Figure. 5, α, β and γ have undergone sufficient learning and adjustment on both datasets, confirming the effectiveness of parameter learnability and demonstrating the heterogeneity of neurons in the network.

Membrane Potential Visualization. We visualize the membrane potential distribution of CTSN neuron models in ResNet20 (trained by TMPR) on CIFAR-100 and CIFAR10-DVS datasets. As observed from Figure. 2, compared to ternary neurons, the distribution of CTSN varies more smoothly over time on both datasets, indicating more stable temporal gradients. Due to the use of the TMPR method for training, the membrane potential distribution demonstrates stronger compactness and symmetry, especially on CIFAR-100 dataset. These results demonstrate that the proposed CTSN and TMPR methods improve the dynamic characteristics of ternary neurons, effectively enhancing model performance by preventing over activation or excessive silence of neurons. Detailed analysis is provided in Appendix D.

6.2. Comparison with SOTA Methods

We evaluate CTSN and TMPR using both static and neuromorphic datasets: CIFAR-10/100 (Krizhevsky et al., 2009) and ImageNet-100 (Deng et al., 2009) are static datasets, while CIFAR10-DVS (Li et al., 2017) is a neuromorphic dataset. Details of training setup and data preprocessing are provided in Appendix G.

Table. 2 reveals that our ternary SNN always outperforms

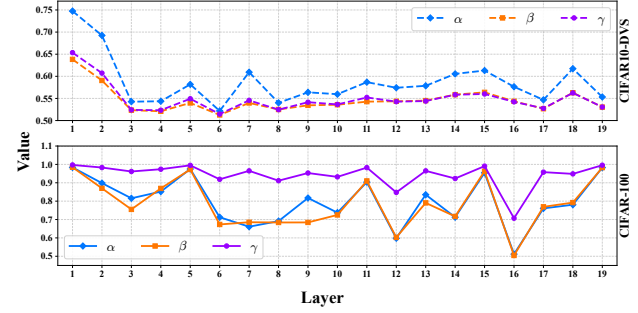


Figure 5. Tracking of learnable parameters in each layer of ResNet20. Upper: Network trained on CIFAR10-DVS with 10 timesteps. Lower: Network trained on CIFAR-100 with 4 timesteps.

the ternary spiking neuron and surpasses all other SNN methods within the same network backbone. Our approach achieves 96.46% accuracy on CIFAR-10 and 81.19% accuracy on CIFAR-100, outperforming other SNN models. On ImageNet-100 dataset, our approach achieves 85.06% accuracy with 4 timesteps, which is a huge improvement compared to other methods. On the widely used neuromorphic dataset CIFAR10-DVS, we compare our approach with other state-of-the-art neuron models. As shown in Table. 2. Our approach scores 79.06% and 81.23%, significantly better than other spiking neuron models. Notably, we implement our approach in open source code and achieve 83.20% using VGGSNN (Deng et al., 2022), indicating its flexibility.

7. Conclusion

In this work, we investigate the problem of iterative information loss, temporal gradient vanishing, and the irregular membrane potential distribution of ternary spiking neurons. We further propose the CTSN model and TMPR method to address these issues. CTSN features additional complemental term in the integration process, which helps to magnify the temporal gradient during backpropagation, retains historical information, and smooths the membrane potential. TMPR method utilizes the complemented membrane potential as regularization, creating extra paths in gradient computation and effectively narrowing the membrane potential distribution. Experimental results demonstrate that the CTSN model with TMPR method achieves state-of-the-art performance in various tasks with different network backbones. Furthermore, the CTSN model exhibits strong biological plausibility, offering great potentials in neuroscience. Nevertheless, due to the mathematical complexity of the CTSN model, a more comprehensive analysis of its neuron dynamic and temporal information transmission mechanisms remains necessary for future work (detailed discussions are provided in Appendix H).

Acknowledgment

This work is supported by the National Natural Science Foundation of China (Grant No. 12401627).

Impact Statement

This paper presents work whose goal is to advance the field of Machine Learning. There are many potential societal consequences of our work, none which we feel must be specifically highlighted here.

References

Capone, C., Lupo, C., Muratore, P., and Paolucci, P. S. Beyond spiking networks: The computational advantages of dendritic amplification and input segregation. *Proceedings of the National Academy of Sciences*, 120(49): e2220743120, 2023.

Cubuk, E. D., Zoph, B., Mané, D., Vasudevan, V., and Le, Q. V. Autoaugment: Learning augmentation strategies from data. In *2019 IEEE/CVF Conference on Computer Vision and Pattern Recognition (CVPR)*, pp. 113–123, 2019.

Deng, J., Dong, W., Socher, R., Li, L.-J., Li, K., and Fei-Fei, L. Imagenet: A large-scale hierarchical image database. In *2009 IEEE conference on computer vision and pattern recognition*, pp. 248–255. Ieee, 2009.

Deng, S., Li, Y., Zhang, S., and Gu, S. Temporal efficient training of spiking neural network via gradient re-weighting. In *International Conference on Learning Representations*, 2022.

DeVries, T. and Taylor, G. W. Improved regularization of convolutional neural networks with cutout. *arXiv preprint arXiv:1708.04552*, 2017.

Ding, Y., Zuo, L., Jing, M., He, P., and Deng, H. Rethinking spiking neural networks from an ensemble learning perspective. In *The Thirteenth International Conference on Learning Representations*, 2025.

Du, K., Wu, Y., Deng, S., and Gu, S. Temporal flexibility in spiking neural networks: Towards generalization across time steps and deployment friendliness. In *The Thirteenth International Conference on Learning Representations*, 2025.

Egorov, A. V., Hamam, B. N., Fransén, E., Hasselmo, M. E., and Alonso, A. A. Graded persistent activity in entorhinal cortex neurons. *Nature*, 420(6912):173–178, 2002.

Fang, W., Yu, Z., Chen, Y., Huang, T., Masquelier, T., and Tian, Y. Deep residual learning in spiking neural networks. *Advances in Neural Information Processing Systems*, 34:21056–21069, 2021a.

Fang, W., Yu, Z., Chen, Y., Masquelier, T., Huang, T., and Tian, Y. Incorporating learnable membrane time constant to enhance learning of spiking neural networks. In *Proceedings of the IEEE/CVF international conference on computer vision*, pp. 2661–2671, 2021b.

Fang, W., Yu, Z., Zhou, Z., Chen, D., Chen, Y., Ma, Z., Masquelier, T., and Tian, Y. Parallel spiking neurons with high efficiency and ability to learn long-term dependencies. *Advances in Neural Information Processing Systems*, 36:53674–53687, 2023.

Feng, S., Feng, W., Gao, X., Zhao, P., and Shen, Z. Ts-lif: A temporal segment spiking neuron network for time series forecasting. In *The Thirteenth International Conference on Learning Representations*, 2025a.

Feng, W., Gao, X., Du, W., Shi, H., Zhao, P., Wu, P., and Miao, C. Efficient parallel training methods for spiking neural networks with constant time complexity. In *Proceedings of the 42nd International Conference on Machine Learning*, volume 267, pp. 16711–16726. PMLR, 2025b.

Gerstner, W., Kistler, W. M., Naud, R., and Paninski, L. *Neuronal dynamics: From single neurons to networks and models of cognition*. Cambridge University Press, 2014.

Guo, Y., Chen, Y., Zhang, L., Wang, Y., Liu, X., Tong, X., Ou, Y., Huang, X., and Ma, Z. Reducing information loss for spiking neural networks. In *European Conference on Computer Vision*, pp. 36–52. Springer, 2022.

Guo, Y., Liu, X., Chen, Y., Zhang, L., Peng, W., Zhang, Y., Huang, X., and Ma, Z. Rmp-loss: Regularizing membrane potential distribution for spiking neural networks. In *Proceedings of the IEEE/CVF International Conference on Computer Vision*, pp. 17391–17401, 2023.

Guo, Y., Chen, Y., Liu, X., Peng, W., Zhang, Y., Huang, X., and Ma, Z. Ternary spike: Learning ternary spikes for spiking neural networks. In *Proceedings of the AAAI conference on artificial intelligence*, volume 38, pp. 12244–12252, 2024.

He, K., Zhang, X., Ren, S., and Sun, J. Deep residual learning for image recognition. In *Proceedings of the IEEE conference on computer vision and pattern recognition*, pp. 770–778, 2016.

Huang, Y., Lin, X., Ren, H., Fu, H., Zhou, Y., Liu, Z., Pan, B., and Cheng, B. Clif: Complementary leaky integrate-and-fire neuron for spiking neural networks. In *International Conference on Machine Learning*, pp. 19949–19972. PMLR, 2024.

Huang, Z., Meng, W., Liu, Q., Chen, K., and Ma, L. Ar-lif: Adaptive reset leaky integrate-and-fire neuron for spiking neural networks. *arXiv preprint arXiv:2507.20746*, 2025.

Isaacson, J. S. and Scanziani, M. How inhibition shapes cortical activity. *Neuron*, 72(2):231–243, 2011.

Krizhevsky, A., Hinton, G., et al. Learning multiple layers of features from tiny images. 2009.

Kudithipudi, D., Schuman, C., Vineyard, C. M., Pandit, T., Merkel, C., Kubendran, R., Aimone, J. B., Orchard, G., Mayr, C., Benosman, R., et al. Neuromorphic computing at scale. *Nature*, 637(8047):801–812, 2025.

Li, H., Liu, H., Ji, X., Li, G., and Shi, L. Cifar10-dvs: an event-stream dataset for object classification. *Frontiers in neuroscience*, 11:309, 2017.

Liu, W., Yang, L., Zhao, M., Wang, S., Gao, J., Li, W., Li, B., and Hu, W. Deeptage: Deep temporal-aligned gradient enhancement for optimizing spiking neural networks. In *The Thirteenth International Conference on Learning Representations*, 2025.

Maass, W. Networks of spiking neurons: the third generation of neural network models. *Neural networks*, 10(9): 1659–1671, 1997.

Meng, Q., Xiao, M., Yan, S., Wang, Y., Lin, Z., and Luo, Z.-Q. Towards memory-and time-efficient backpropagation for training spiking neural networks. In *Proceedings of the IEEE/CVF international conference on computer vision*, pp. 6166–6176, 2023.

Mukhoty, B., Bojkovic, V., de Vazelhes, W., Zhao, X., De Masi, G., Xiong, H., and Gu, B. Direct training of snn using local zeroth order method. *Advances in Neural Information Processing Systems*, 36:18994–19014, 2023.

Neftci, E. O., Mostafa, H., and Zenke, F. Surrogate gradient learning in spiking neural networks: Bringing the power of gradient-based optimization to spiking neural networks. *IEEE Signal Processing Magazine*, 36(6):51–63, 2019.

Rathi, N. and Roy, K. Diet-snn: A low-latency spiking neural network with direct input encoding and leakage and threshold optimization. *IEEE Transactions on Neural Networks and Learning Systems*, 34(6):3174–3182, 2021.

Roy, K., Jaiswal, A., and Panda, P. Towards spike-based machine intelligence with neuromorphic computing. *Nature*, 575(7784):607–617, 2019.

Rumelhart, D. E., Hinton, G. E., and Williams, R. J. Learning representations by back-propagating errors. *nature*, 323(6088):533–536, 1986.

Schmidt, M., Bakker, R., Shen, K., Bezgin, G., Diesmann, M., and van Albada, S. J. A multi-scale layer-resolved spiking network model of resting-state dynamics in macaque visual cortical areas. *PLoS Computational Biology*, 14(10):e1006359, 2018.

Schuman, C. D., Kulkarni, S. R., Parsa, M., Mitchell, J. P., Date, P., and Kay, B. Opportunities for neuromorphic computing algorithms and applications. *Nature Computational Science*, 2(1):10–19, 2022.

Shen, H., Zheng, Q., Wang, H., and Pan, G. Rethinking the membrane dynamics and optimization objectives of spiking neural networks. *Advances in Neural Information Processing Systems*, 37:92697–92720, 2024.

Siegle, J. H., Jia, X., Durand, S., Gale, S., Bennett, C., Graddis, N., Heller, G., Ramirez, T. K., Choi, H., Luviano, J. A., et al. Survey of spiking in the mouse visual system reveals functional hierarchy. *Nature*, 592(7852):86–92, 2021.

Simonyan, K. and Zisserman, A. Very deep convolutional networks for large-scale image recognition. In *International Conference on Learning Representations*, 2015.

Sun, C., Chen, Q., Fu, Y., and Li, L. Deep spiking neural network with ternary spikes. In *2022 IEEE Biomedical Circuits and Systems Conference (BioCAS)*, pp. 251–254. IEEE, 2022.

Turrigiano, G. G. The self-tuning brain: Cortical plasticity during sleep and wakefulness. *Cell*, 135(3):422–435, 2008.

Wang, K., Chou, Y., Shang, D., Mei, S., Zhang, J., Huang, Y., Yao, M., Xu, B., and Li, G. Mmdend: Dendrite-inspired multi-branch multi-compartment parallel spiking neuron for sequence modeling. In *Proceedings of the 63rd Annual Meeting of the Association for Computational Linguistics (Volume 1: Long Papers)*, pp. 27459–27470, 2025.

Wang, S., Cheng, T. H., and Lim, M.-H. Ltmd: learning improvement of spiking neural networks with learnable thresholding neurons and moderate dropout. *Advances in Neural Information Processing Systems*, 35:28350–28362, 2022.

Wang, Z., Jiang, R., Lian, S., Yan, R., and Tang, H. Adaptive smoothing gradient learning for spiking neural networks. In *International conference on machine learning*, pp. 35798–35816. PMLR, 2023.

Wolff, A., Berberian, N., Golesorkhi, M., Gomez-Pilar, J., Zilio, F., and Northoff, G. Intrinsic neural timescales: temporal integration and segregation. *Trends in cognitive sciences*, 26(2):159–173, 2022.

Wu, Y., Deng, L., Li, G., Zhu, J., and Shi, L. Spatio-temporal backpropagation for training high-performance spiking neural networks. *Frontiers in Neuroscience*, 12: 331, 2018.

Wu, Y., Deng, L., Li, G., Zhu, J., Xie, Y., and Shi, L. Direct training for spiking neural networks: Faster, larger, better. In *Proceedings of the AAAI conference on artificial intelligence*, volume 33, pp. 1311–1318, 2019.

Xue, M., Atallah, B. V., and Scanziani, M. Equalization of excitation–inhibition ratios across the entire frequency range. *Nature*, 511(7511):596–600, 2014.

Yao, X., Li, F., Mo, Z., and Cheng, J. Glif: A unified gated leaky integrate-and-fire neuron for spiking neural networks. *Advances in Neural Information Processing Systems*, 35:32160–32171, 2022.

Zhang, B., Xu, Z., and Tao, K. Temporal regularization training: Unleashing the potential of spiking neural networks. *arXiv preprint arXiv:2506.19256*, 2026.

Zheng, H., Wu, Y., Deng, L., Hu, Y., and Li, G. Going deeper with directly-trained larger spiking neural networks. In *Proceedings of the AAAI conference on artificial intelligence*, volume 35, pp. 11062–11070, 2021a.

Zheng, H., Wu, Y., Deng, L., Hu, Y., and Li, G. Going deeper with directly-trained larger spiking neural networks. In *Proceedings of the AAAI conference on artificial intelligence*, volume 35, pp. 11062–11070, 2021b.

Zheng, H., Zheng, Z., Hu, R., Xiao, B., Wu, Y., Yu, F., Liu, X., Li, G., and Deng, L. Temporal dendritic heterogeneity incorporated with spiking neural networks for learning multi-timescale dynamics. *Nature Communications*, 15 (1):277, 2024.

A. Detailed Discussion on Inspired Biological Principles

The design of CTSN draws its inspiration primarily from the core characteristics of the biological nervous system across both spatial and temporal dimensions.

On spatial dimension, the design originates from the excitation-inhibition balance mechanism. In biology, the functional homeostasis of neural circuits depends on a precise and constant ratio between excitatory and inhibitory inputs (Xue et al., 2014). This property is crucial for information processing in the cerebral cortex, preventing epileptiform discharges caused by excessive excitation while avoiding functional silence due to excessive inhibition (Turriagano, 2008). The critical biological mechanism relies on the dynamic interaction between excitatory pyramidal neurons and inhibitory GABAergic interneurons: inhibitory neurons constrain the temporal window for synaptic integration through feedforward inhibition, thereby enforcing instantaneous fidelity in spike timing and sharpening the spatial tuning capabilities of cortical neurons (Isaacson & Scanziani, 2011). Ternary spiking neurons (Guo et al., 2024) are capable to mimic this mechanism by generating 1 and -1 spikes that simulate excitatory and inhibitory signals respectively. CTSN inherits this bio-inspired feature.

On temporal dimension, neurons possess complex temporal integration capabilities. Neurons in the cerebral cortex exhibit hierarchical sustained activity, whereby neurons convert the intensity of previous inputs into a sustained depolarized membrane potential state lasting several seconds, even in the absence of continuous synaptic input (Egorov et al., 2002). More than that, neurons exhibit strong temporal heterogeneity (Wolff et al., 2022). Neural activities in different regions of the human brain have different timescales. Different neurons possess distinct time windows for information processing. Inspired by these two mechanisms, CTSN introduces a non-resetting adaptive memory term $h(t)$ to simulate the hierarchical sustained activity and heterogeneity of biological neurons. When processing input signals, CTSN records and maintains the membrane potential state from previous timesteps while adaptively adjusts the memory strength.

B. Performance of the Ternary Spiking Neuron with Soft Reset Mechanism

As discussed in Section 4.1, the soft reset mechanism is usually implemented to address the iterative information loss issue on binary spiking neurons. To explore this mechanism on ternary spiking neuron, we conduct experiments on CIFAR-100 and CIFAR10-DVS datasets. The membrane potential of ternary spiking neuron with soft reset mechanism updates as

$$u(t) = \tau(u(t-1) - o(t-1)V_{th}) + x(t). \quad (26)$$

For ResNet20 on CIFAR10-DVS, we visualize the membrane potential distribution of these two kind of ternary spiking neurons in Figure. 6 as an example. The results in Table. 3 show that the soft-resetting ternary spiking neuron performs worse than the hard-resetting version on both datasets, indicating that the soft reset mechanism is not suitable for ternary spiking neurons. We argue that this is due to the fact that the ternary spiking neuron is capable of emitting both positive and negative spikes. The spiking regions of its membrane potential ($(-\infty, -V_{th}]$ and $[V_{th}, +\infty)$) are symmetric about zero. As shown in the left part of Figure. 6, the distribution of the hard-resetting neurons is sharply peaked. Due to the hard reset mechanism, the membrane potential will always be reset to zero, which is the midpoint of its spiking regions. On the contrary, although the distribution of the soft-resetting neurons is smoother, the soft reset mechanism forces the neuron to retain the residual potentials, which destroys the symmetry of the membrane potential. For example, for a soft-resetting neuron with $V_{th} = 0.5$, membrane potential $u(t) = 2.5$ will be reset to 2.0 at $t + 1$, which will still trigger a spike. As shown in the right part of Figure. 6, a large number of membrane potentials within the extensive spiking regions cannot be reset to zero after each spike emitted, which may lead to excessive neural activation in subsequent stages, resulting in performance degradation.

Table 3. Comparative accuracy of ternary spiking ResNet20 with different reset mechanisms (%).

Dataset	T	Reset Mechanism	
		Hard	Soft
CIFAR-100	4	73.95	73.56
CIFAR10-DVS	10	80.30	80.20

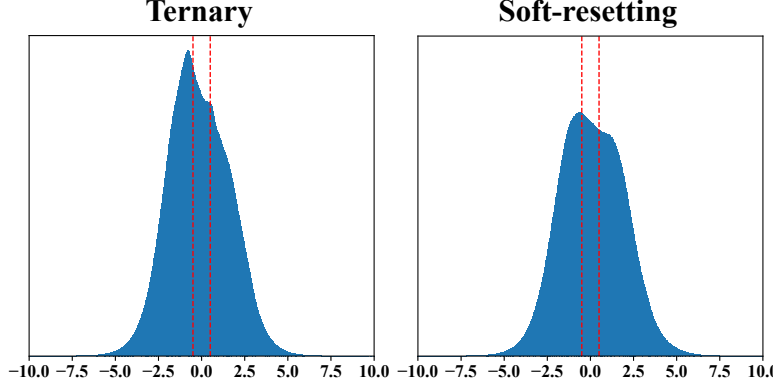


Figure 6. Membrane potential Distributions for the third layer of ResNet20 across all timesteps. Left: Hard-resetting neuron. Right: Soft-resetting neuron. Dashed lines indicate the spiking thresholds.

C. BPTT for Ternary Spiking Neuron with Surrogate Gradient

This section is mainly referenced from (Wu et al., 2018; Meng et al., 2023; Huang et al., 2024). Firstly, we recall the ternary spiking neuron model defined in Eq. 1 - 3 and rewrite this model as

$$u^l(t) = \tau u^l(t-1)(1 - |o^l(t-1)|) + \sum_{l=1}^L \mathbf{W}^l o^{l-1}(t) + b^l, \quad (27)$$

and

$$\begin{aligned} o^l(t) &= \Theta(u^l(t), V_{th}) \\ &= \begin{cases} 1, & \text{if } u^l(t) \geq V_{th} \\ -1, & \text{if } u^l(t) \leq -V_{th} \\ 0, & \text{otherwise} \end{cases}. \end{aligned} \quad (28)$$

As described in Section 4.2, the gradient of loss function \mathcal{L} with respect to weight matrix \mathbf{W}^l is calculated as

$$\frac{\partial \mathcal{L}}{\partial \mathbf{W}^l(t)} = \sum_{t=1}^T \frac{\partial \mathcal{L}}{\partial u^l(t)} \frac{\partial u^l(t)}{\partial \mathbf{W}^l(t)}, \quad (29)$$

where \mathcal{L} represents the loss function. The partial derivative $\frac{\partial \mathcal{L}}{\partial u^l(t)}$ can be recursively calculated as

$$\frac{\partial \mathcal{L}}{\partial u^l(t)} = \frac{\partial \mathcal{L}}{\partial o^l(t)} \frac{\partial o^l(t)}{\partial u^l(t)} + \frac{\partial \mathcal{L}}{\partial u^l(t+1)} \epsilon^l(t), \quad (30)$$

where $\epsilon^l(t)$ is defined as

$$\epsilon^l(t) \equiv \frac{\partial u^l(t+1)}{\partial u^l(t)} + \frac{\partial u^l(t+1)}{\partial |o^l(t)|} \frac{\partial |o^l(t)|}{\partial u^l(t)}. \quad (31)$$

In this case, we calculate the gradient term $\frac{\partial \mathcal{L}}{\partial u^l(t)}$ recursively:

$$\begin{aligned}
 \frac{\partial \mathcal{L}}{\partial u^l(t)} &= \frac{\partial \mathcal{L}}{\partial o^l(t)} \frac{\partial o^l(t)}{\partial u^l(t)} + \frac{\partial \mathcal{L}}{\partial u^l(t+1)} \epsilon^l(t) \\
 &= \frac{\partial \mathcal{L}}{\partial o^l(t)} \frac{\partial o^l(t)}{\partial u^l(t)} + \left(\frac{\partial \mathcal{L}}{\partial o^l(t+1)} \frac{\partial o^l(t+1)}{\partial u^l(t+1)} + \frac{\partial \mathcal{L}}{\partial u^l(t+2)} \epsilon^l(t+1) \right) \epsilon^l(t) \\
 &= \frac{\partial \mathcal{L}}{\partial o^l(t)} \frac{\partial o^l(t)}{\partial u^l(t)} + \frac{\partial \mathcal{L}}{\partial o^l(t+1)} \frac{\partial o^l(t+1)}{\partial u^l(t+1)} \epsilon^l(t) + \frac{\partial \mathcal{L}}{\partial u^l(t+2)} \epsilon^l(t+1) \epsilon^l(t) \\
 &= \frac{\partial \mathcal{L}}{\partial o^l(t)} \frac{\partial o^l(t)}{\partial u^l(t)} + \frac{\partial \mathcal{L}}{\partial o^l(t+1)} \frac{\partial o^l(t+1)}{\partial u^l(t+1)} \epsilon^l(t) + \left(\frac{\partial \mathcal{L}}{\partial o^l(t+2)} \frac{\partial o^l(t+2)}{\partial u^l(t+2)} + \frac{\partial \mathcal{L}}{\partial u^l(t+3)} \epsilon^l(t+2) \right) \epsilon^l(t+1) \epsilon^l(t) \\
 &= \frac{\partial \mathcal{L}}{\partial o^l(t)} \frac{\partial o^l(t)}{\partial u^l(t)} + \frac{\partial \mathcal{L}}{\partial o^l(t+1)} \frac{\partial o^l(t+1)}{\partial u^l(t+1)} \epsilon^l(t) + \frac{\partial \mathcal{L}}{\partial o^l(t+2)} \frac{\partial o^l(t+2)}{\partial u^l(t+2)} \epsilon^l(t+1) \epsilon^l(t) \\
 &\quad + \frac{\partial \mathcal{L}}{\partial u^l(t+3)} \epsilon^l(t+2) \epsilon^l(t+1) \epsilon^l(t) \\
 &\dots \\
 &= \frac{\partial \mathcal{L}}{\partial o^l(t)} \frac{\partial o^l(t)}{\partial u^l(t)} + \sum_{t'=t+1}^T \frac{\partial \mathcal{L}}{\partial o^l(t')} \frac{\partial o^l(t')}{\partial u^l(t')} \prod_{t''=1}^{t'-t} \epsilon^l(t' - t''),
 \end{aligned} \tag{32}$$

which is consistent with Eq. 7.

When $t = T$, the recursive part does not exist and Eq. 32 reduces to

$$\frac{\partial \mathcal{L}}{\partial u^l(T)} = \frac{\partial \mathcal{L}}{\partial o^l(T)} \frac{\partial o^l(T)}{\partial u^l(T)}. \tag{33}$$

For intermediate layers $l = L-1, L-2, \dots, 1$ in SNN, the gradient term $\frac{\partial \mathcal{L}}{\partial u^l(t)}$ is obtained from the previous layer during backpropagation. Therefore, $\frac{\partial \mathcal{L}}{\partial u^l(t)}$ can be rewritten as

$$\frac{\partial \mathcal{L}}{\partial u^l(t)} = \frac{\partial \mathcal{L}}{\partial u^{l+1}(t)} \frac{\partial u^{l+1}(t)}{\partial o^l(t)} \frac{\partial o^l(t)}{\partial u^l(t)} + \sum_{t'=t+1}^T \frac{\partial \mathcal{L}}{\partial u^{l+1}(t')} \frac{\partial u^{l+1}(t')}{\partial o^l(t')} \frac{\partial o^l(t')}{\partial u^l(t')} \prod_{t''=1}^{t'-t} \epsilon^l(t' - t''). \tag{34}$$

As for the last layer $l = L$ of SNN, the gradient term $\frac{\partial \mathcal{L}}{\partial u^L(t)}$ is obtained directly from the loss function during backpropagation. Therefore, $\frac{\partial \mathcal{L}}{\partial u^L(t)}$ remains consistent with Eq. 32:

$$\frac{\partial \mathcal{L}}{\partial u^L(t)} = \frac{\partial \mathcal{L}}{\partial o^L(t)} \frac{\partial o^L(t)}{\partial u^L(t)} + \sum_{t'=t+1}^T \frac{\partial \mathcal{L}}{\partial o^L(t')} \frac{\partial o^L(t')}{\partial u^L(t')} \prod_{t''=1}^{t'-t} \epsilon^L(t' - t''). \tag{35}$$

The Eq. 34 and Eq. 35 corresponds to Eq. 7 and Eq. 8.

D. Visualization of the Membrane Potential

In this section, we provide detailed visualization of the membrane potential distributions for ResNet20. As observed from the Figure. 7, the distribution of ternary spiking neurons gradually derives into a bimodal pattern when processing static image data, but maintains sharply peaked unimodal distribution on neuromorphic data. As shown in Figure. 8, the distribution of CTSN models varies more smoothly over time. On CIFAR-100 dataset, the distribution starts to derive into bimodal patterns on the first timestep, which is earlier than ternary spiking neurons. On CIFAR10-DVS dataset, the membrane potential exhibits stronger smoothness. Furthermore, the membrane potential distribution exhibits stronger compactness and symmetry, especially on CIFAR-100 dataset. These results indicate that the proposed CTSN and TMPR methods effectively improve neuron dynamics, preventing membrane potentials from excessively residing in activation regions far from the threshold or in silent regions near zero, thereby avoiding over activation or excessive silence.

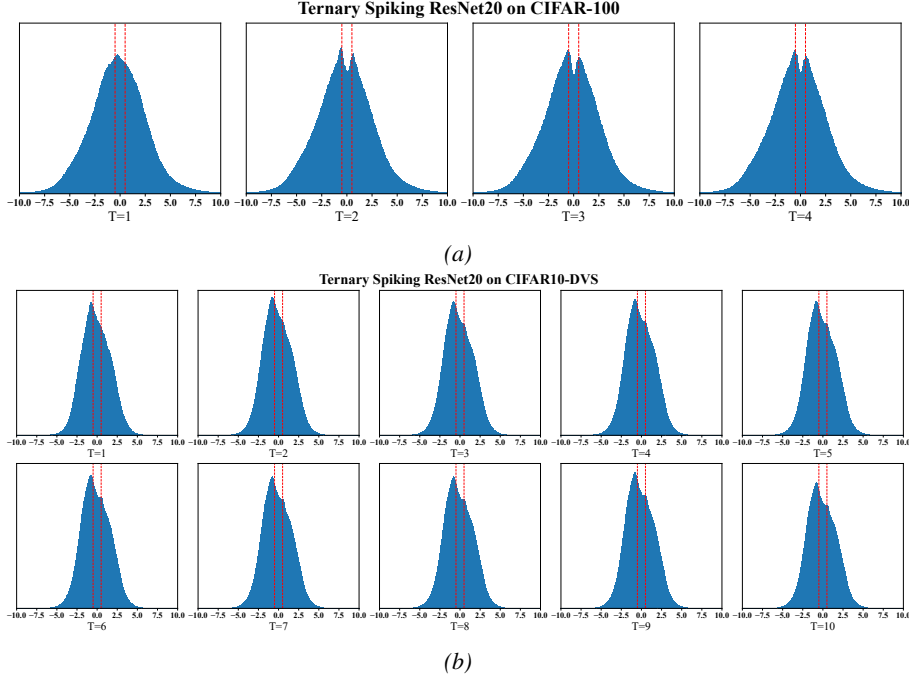


Figure 7. Membrane potential Distributions for the third layer of Ternary Spiking ResNet20. (a) CIFAR-100. (b) CIFAR10-DVS.

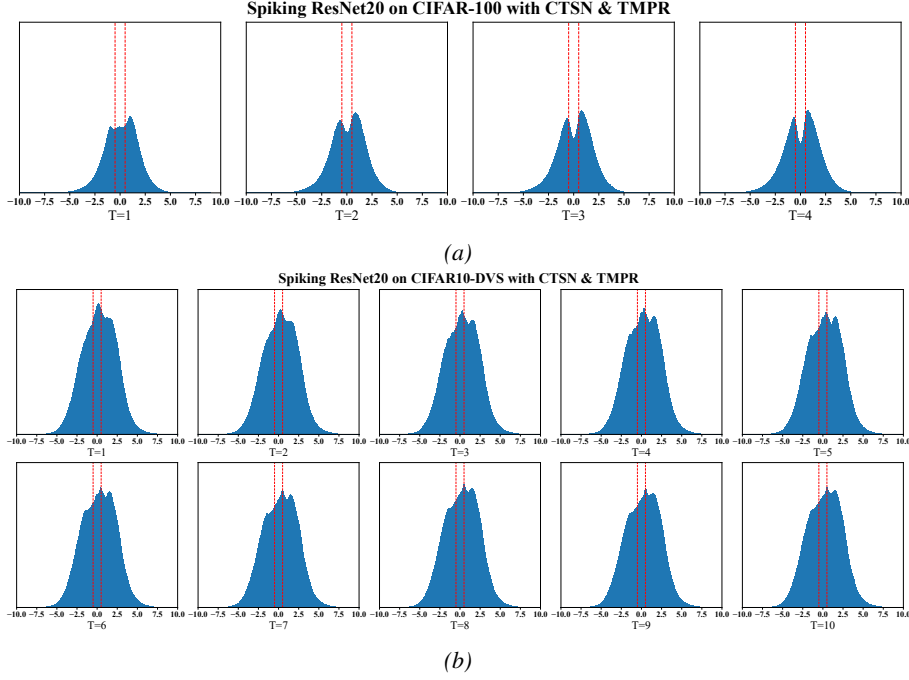


Figure 8. Membrane potential Distributions for the third layer of CTSN Spiking ResNet20 trained by TMPR. (a) CIFAR-100. (b) CIFAR10-DVS.

E. Pseudo-code for Proposed Methods

E.1. Pseudo-code for the CTSN Model

The pseudo-code for the CTSN method is shown in Algorithm. 1.

Algorithm 1 Core Function of CTSN Model.

Input: data \mathbf{x} , total timesteps T , time constant τ , threshold V_{th} , learnable parameters α, β, γ , data type.
Output: spike sequence \mathcal{S} and membrane potential train \mathcal{U} .
Initial: $\mathbf{u}(t) = 0, \mathbf{h}(t) = 0, \tilde{\mathbf{u}}(t) = 0, \mathcal{S} = \{\}, \mathcal{U} = \{\}$.
for $t = 1, \dots, T$ **do**
 $\mathbf{u}(t) = \tau \tilde{\mathbf{u}}(t)$;
 if processing static data **then**
 $\mathbf{h}(t) = \alpha \text{ReLU}(\mathbf{h}(t-1)) + \beta(-\text{ReLU}(-\mathbf{h}(t-1))) + \gamma \mathbf{u}(t)$;
 end if
 if processing neuromorphic data **then**
 $\mathbf{h}(t) = \alpha \mathbf{h}(t-1) + \beta \text{ReLU}(\mathbf{u}(t)) + \gamma(-\text{ReLU}(-\mathbf{u}(t)))$;
 end if
 $\tilde{\mathbf{u}}(t) = \mathbf{h}(t) + \mathbf{x}(t)$;
 $\mathcal{U} \cup \tilde{\mathbf{u}}(t)$;
 $\mathbf{o}(t) = \Theta(\tilde{\mathbf{u}}(t), V_{th})$;
 $\mathcal{S} \cup \mathbf{o}(t)$;
 $\tilde{\mathbf{u}}(t) = \tilde{\mathbf{u}}(t)(1 - |\mathbf{o}(t)|)$;
end for
Return: \mathcal{S}, \mathcal{U} .

E.2. Pseudo-code for the TMPR Training Method

The pseudo-code for the TMPR training method is shown in Algorithm. 2.

Algorithm 2 Training an SNN with TMPR Method.

Input: SNN model, total timesteps T , training data, total number of training epochs N , number of training batches in one epoch B , layer number of the SNN model L , regularization coefficient λ .
Output: trained SNN model.
for $n = 1, \dots, N$ **do**
 for $i = 1, \dots, B$ **do**
 Get training data, and class label: \mathbf{Y}^i ;
 Compute the SNN output \mathbf{O}^i ;
 Compute classification loss $\mathcal{L}_{\text{CE}} = \mathcal{L}_{\text{CE}}(\mathbf{O}^i, \mathbf{Y}^i)$;
 Initialize \mathbf{U}^i to 0;
 for $l = 1, \dots, L$ **do**
 Get and store each layer's flatten membrane potential of each timestep into \mathbf{U}^i ;
 end for
 Compute TMPR loss $\mathcal{L}_{\text{TMPR}}$ based on Eq. 20 using \mathbf{U}^i and λ ;
 Compute the total loss $\mathcal{L} = \mathcal{L}_{\text{CE}} + \mathcal{L}_{\text{TMPR}}$;
 Backpropagation and update model parameters;
 end for
end for
Return: The trained SNN model.

F. The Gradients of CTSN

The proposed CTSN model defined by Eq. 12 - 17 can be rewritten as

$$h^l(t) = \mathbb{G}\left(h^l(t-1), \tau \tilde{u}^l(t-1)(1 - |\mathbf{o}^l(t-1)|), \alpha^l, \beta^l, \gamma^l\right), \quad (36)$$

$$\tilde{u}^l(t) = h^l(t) + \sum_{l=1}^L \mathbf{W}^l \mathbf{o}^{l-1}(t) + b^l, \quad (37)$$

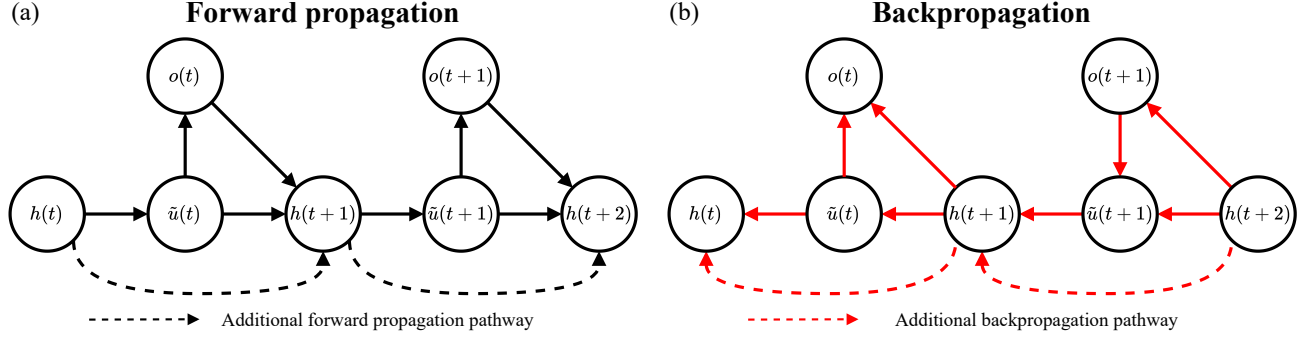


Figure 9. The computation graph of (a) forward propagation and (b) backpropagation for CTSN model.

and

$$o^l(t) = \Theta(\tilde{u}^l(t), V_{th}). \quad (38)$$

The function \mathbb{G} for static image data can be rewritten as

$$\mathbb{G}(h(t-1), u, \alpha, \beta, \gamma) = \alpha \text{ReLU}(h(t-1)) + \beta(-\text{ReLU}(-h(t-1))) + \gamma u. \quad (39)$$

The function \mathbb{G} for neuromorphic data can be rewritten as

$$\mathbb{G}(h(t-1), u, \alpha, \beta, \gamma) = \alpha h(t-1) + \beta \text{ReLU}(u) + \gamma(-\text{ReLU}(-u)). \quad (40)$$

We define function $\text{Choice}(x, v_{th}, a, b)$ as

$$\text{Choice}(x, v_{th}, a, b) = \begin{cases} a, & x \geq v_{th} \\ b, & x < v_{th} \end{cases}. \quad (41)$$

The gradient term $\frac{\partial \mathcal{L}}{\partial \tilde{u}^l(t)}$ can be recursively calculated as

$$\frac{\partial \mathcal{L}}{\partial \tilde{u}^l(t)} = \frac{\partial \mathcal{L}}{\partial o^l(t)} \frac{\partial o^l(t)}{\partial \tilde{u}^l(t)} + \frac{\partial \mathcal{L}}{\partial \tilde{u}^l(t+1)} \frac{\partial \tilde{u}^l(t+1)}{\partial h^l(t+1)} \xi^l(t), \quad (42)$$

where $\xi^l(t)$ is expanded as

$$\begin{aligned} \xi^l(t) &= \frac{\partial h^l(t+1)}{\partial \tilde{u}^l(t)} + \frac{\partial h^l(t+1)}{\partial |o(t)|} \frac{\partial |o(t)|}{\partial \tilde{u}^l(t)} \\ &= \nabla_{\tilde{u}^l} \mathbb{G}^l + \frac{\partial h^l(t+1)}{\partial |o(t)|} \frac{\partial |o(t)|}{\partial \tilde{u}^l(t)}. \end{aligned} \quad (43)$$

From Eq. 39 and Eq. 40, $\nabla_{\tilde{u}^l} \mathbb{G}^l$ is calculated as

$$\nabla_{\tilde{u}^l} \mathbb{G}^l = \begin{cases} \gamma^l, & \text{static} \\ \text{Choice}(\tilde{u}^l, 0, \beta^l, \gamma^l), & \text{neuromorphic} \end{cases}. \quad (44)$$

To better understand Eq. 42, Eq. 43 and the following derivation, we refer to Figure 9. In this case, we calculate the gradient term $\frac{\partial \mathcal{L}}{\partial \tilde{u}^l(t)}$ recursively:

$$\begin{aligned}
 \frac{\partial \mathcal{L}}{\partial \tilde{u}^l(t)} &= \frac{\partial \mathcal{L}}{\partial o^l(t)} \frac{\partial o^l(t)}{\partial \tilde{u}^l(t)} + \frac{\partial \mathcal{L}}{\partial \tilde{u}^l(t+1)} \underbrace{\frac{\partial \tilde{u}^l(t+1)}{\partial h^l(t+1)} \xi^l(t)}_{=1} \\
 &= \frac{\partial \mathcal{L}}{\partial o^l(t)} \frac{\partial o^l(t)}{\partial \tilde{u}^l(t)} + \frac{\partial \mathcal{L}}{\partial \tilde{u}^l(t+1)} \xi^l(t) \\
 &= \frac{\partial \mathcal{L}}{\partial o^l(t)} \frac{\partial o^l(t)}{\partial \tilde{u}^l(t)} + \left(\frac{\partial \mathcal{L}}{\partial o^l(t+1)} \frac{\partial o^l(t+1)}{\partial \tilde{u}^l(t+1)} + \frac{\partial \mathcal{L}}{\partial \tilde{u}^l(t+2)} \underbrace{\frac{\partial \tilde{u}^l(t+2)}{\partial h^l(t+2)} (\xi^l(t+1) + \frac{\partial h^l(t+2)}{\partial h^l(t+1)})}_{=1} \right) \xi^l(t) \\
 &= \frac{\partial \mathcal{L}}{\partial o^l(t)} \frac{\partial o^l(t)}{\partial \tilde{u}^l(t)} + \frac{\partial \mathcal{L}}{\partial o^l(t+1)} \frac{\partial o^l(t+1)}{\partial \tilde{u}^l(t+1)} \xi^l(t) + \frac{\partial \mathcal{L}}{\partial \tilde{u}^l(t+2)} (\xi^l(t+1) + \nabla_{h^l} \mathbb{G}^l) \xi^l(t) \\
 &= \frac{\partial \mathcal{L}}{\partial o^l(t)} \frac{\partial o^l(t)}{\partial \tilde{u}^l(t)} + \frac{\partial \mathcal{L}}{\partial o^l(t+1)} \frac{\partial o^l(t+1)}{\partial \tilde{u}^l(t+1)} \xi^l(t) \\
 &\quad + \left(\frac{\partial \mathcal{L}}{\partial o^l(t+2)} \frac{\partial o^l(t+2)}{\partial \tilde{u}^l(t+2)} + \frac{\partial \mathcal{L}}{\partial \tilde{u}^l(t+3)} \underbrace{\frac{\tilde{u}^l(t+3)}{h^l(t+3)} (\xi^l(t+2) + \frac{\partial h(t+3)}{\partial h(t+2)})}_{=1} \right) \cdot (\xi^l(t+1) + \nabla_{h^l} \mathbb{G}^l) \xi^l(t) \\
 &= \frac{\partial \mathcal{L}}{\partial o^l(t)} \frac{\partial o^l(t)}{\partial \tilde{u}^l(t)} + \frac{\partial \mathcal{L}}{\partial o^l(t+1)} \frac{\partial o^l(t+1)}{\partial \tilde{u}^l(t+1)} \xi^l(t) \\
 &\quad + \frac{\partial \mathcal{L}}{\partial o^l(t+2)} \frac{\partial o^l(t+2)}{\partial \tilde{u}^l(t+2)} (\xi^l(t+1) + \nabla_{h^l} \mathbb{G}^l) \xi^l(t) \\
 &\quad + \frac{\partial \mathcal{L}}{\partial \tilde{u}^l(t+3)} \frac{\tilde{u}^l(t+3)}{h^l(t+3)} (\xi^l(t+2) + \nabla_{h^l} \mathbb{G}^l) (\xi^l(t+1) + \nabla_{h^l} \mathbb{G}^l) \xi^l(t) \\
 &\quad \dots \\
 &= \frac{\partial \mathcal{L}}{\partial o^l(t)} \frac{\partial o^l(t)}{\partial \tilde{u}^l(t)} + \frac{\partial \mathcal{L}}{\partial o^l(t+1)} \frac{\partial o^l(t+1)}{\partial \tilde{u}^l(t+1)} \xi^l(t) + \sum_{t'=t+2}^T \left(\frac{\partial \mathcal{L}}{\partial o^l(t')} \frac{\partial o^l(t')}{\partial \tilde{u}^l(t')} \prod_{t''=1}^{t'-t} (\xi^l(t' - t'') + \underbrace{\nabla_{h^l} \mathbb{G}^l}_{\text{Complemental Gradient}}) \right),
 \end{aligned} \tag{45}$$

where $\nabla_{h^l} \mathbb{G}^l$ can be calculated as

$$\nabla_{h^l} \mathbb{G}^l = \begin{cases} \text{Choice}(h^l, 0, \alpha^l, \beta^l), & \text{static} \\ \alpha^l, & \text{neuromorphic} \end{cases}. \tag{46}$$

Similar to the ternary spiking neuron, in CTSN model we have

$$\frac{\partial \mathcal{L}}{\partial o^l(t)} = \begin{cases} \frac{\partial \mathcal{L}}{\partial o^L(t)}, & l = L \\ \frac{\partial \mathcal{L}}{\partial u^{l+1}(t)} \frac{\partial u^{l+1}(t)}{\partial o^l(t)}, & l = L-1, L-2 \dots 1 \end{cases}. \tag{47}$$

From Eq. 45, we can intuitively see that the additional term of CTSN magnifies the temporal gradient, which akin to taking a shortcut on the temporal dimension, mitigating the temporal gradient vanishing issue caused by the product operations.

G. Experiment Description and Dataset Pre-processing

Unless otherwise specified or for the purpose of comparative experiments, the experiments in this paper employ the following configurations and data preprocessing procedures: all our self-implementations use rectangle-shaped surrogate functions with $a = V_{th} = 0.5$, the time constant τ is set to 0.25. Except the experiments with TMPR, we use cross-entropy as the loss function. All the experiments are based on the PyTorch framework and conducted on NVIDIA RTX 4090D GPUs. The default configurations are listed in Table. 4 and the detailed dataset descriptions are provided in the following sections.

Table 4. Training hyperparameters. *: Momentum is set to 0.9. †: Decay to 0 via cosine annealing strategy.

Dataset	Optimizer*	Weight Decay	Batch Size	Epoch	Learning Rate [†]
CIFAR-10	SGD	1e-4	64	300	0.1
CIFAR-100	SGD	1e-4	64	300	0.1
ImageNet100	SGD	1e-4	64	300	0.1
CIFAR10-DVS	SGD	5e-4	64	300	0.1

CIFAR-10/100. Both CIFAR-10 and CIFAR-100 (Krizhevsky et al., 2009) datasets contain 60,000 32×32 color images corresponding to 10 and 100 categories, respectively. Each dataset includes 50,000 training samples and 10,000 test samples. We apply normalization to all image data to make sure input images have 0 mean and 1 variance. We conduct random horizontal flipping and cropping on training data to avoid overfitting. The AutoAugment (Cubuk et al., 2019) and Cutout (DeVries & Taylor, 2017) are also applied for data augmentation. Direct encoding (Rathi & Roy, 2021) is employed to encode image data into time series. For the CIFAR classification task, we use ResNet19 and ResNet20 (He et al., 2016) as backbones.

ImageNet-100. ImageNet-100 is a commonly used subset of the full ImageNet dataset (Deng et al., 2009), comprising 100 categories. This subset typically contains approximately 130,000 images, with the training set holding roughly 126,000 images and the validation set holding about 5,000 images. All images were uniformly resized to 224×224 pixels prior to processing. We apply random horizontal flipping and cropping to training images, while the center cropping is applied to validation images. Consistent with the CIFAR datasets, we utilize the direct encoding to encode image data into time series. For the ImageNet-100 classification task, we use ResNet34 and SEW-ResNet34 (Fang et al., 2021a) as backbones.

CIFAR10-DVS. The CIFAR10-DVS dataset (Li et al., 2017) is a neuromorphic dataset generated by recording object motion from CIFAR-10 using dynamic visual sensors (DVS). It contains 10,000 event stream samples with an original spatial resolution of 128×128 pixels. In this work, we split the dataset at a 9:1 ratio into 9k training samples and 1k test samples. All event frames are preprocessed and resized to 48×48 pixels. Following Deng et al. (2022), we take random horizontal flipping and random roll within 5 pixels as augmentation for training data. For CIFAR10-DVS, we use ResNet20 and VGG16 (Simonyan & Zisserman, 2015) as backbones.

H. Discussion and Limitation

Flexibility. A key advantage of our algorithms are their flexibility. Both CTSN and TMPR impose no constraints on specific network architectures, ensuring their general applicability across various SNN models.

Application Prospects. The depolarization-like mechanism provided by the complemental term and the ternary spiking characteristic offers CTSN great biological plausibility, making CTSN a highly potential framework for modeling neural activities in computational neuroscience. The TMPR method is a practical and powerful approach for pretraining ternary SNNs, and it can potentially be extended to binary SNNs, providing high-performance pre-trained SNN models for various application scenarios.

Limitations. For different types of inputs, CTSN exhibits distinct neuron behaviors, making it a model lacks of generality. Due to the characteristic of emitting both positive and negative spikes, CTSN model generate spikes more frequently than binary neurons, resulting in higher energy consumption. Moreover, this characteristic leads to poor compatibility with existing neuromorphic hardware designed for binary neurons. Nevertheless, CTSN model and TMPR method introduce additional operations to membrane potentials, which inevitably reduce computational efficiency in training period.

Future Outlooks. The underlying principles governing neuron dynamics and temporal information transmission mechanisms of both ternary spiking neuron and CTSN model are not yet fully understood, which require further study in the future. It is necessary to develop ternary spiking neuron models with higher generality to various types of inputs. Furthermore, to lower costs in real-world application scenarios, it is crucial to develop ternary spiking neuron models and training methods that offer higher computational and energy efficiency, as well as compatibility with neuromorphic hardware.